

Dynamic Mode Decomposition of the Core-surface Flow

Jinfeng Li¹, Yufeng Lin¹

¹Department of Earth and Space Sciences, Southern University of Science and Technology, Shenzhen 518055, China

1 Dynamic Mode Decomposition

The dynamic mode decomposition (DMD) is a well-established method for decomposing temporal snapshots or measurements of a system into a set of dynamics modes. Here we introduce a concise procedure for the core-surface flow decomposition using DMD. Our core flow model offers two sets of flow snapshots spanning the year 2000 to 2019 and 2001 to 2020, respectively. Each set comprises snapshots represented as

$$\mathbf{X} = (\mathbf{x}_{2000}, \mathbf{x}_{2001}, \dots, \mathbf{x}_{2019}) \in \mathbb{R}^{n \times m}, \quad (1)$$

$$\mathbf{X}' = (\mathbf{x}_{2001}, \mathbf{x}_{2002}, \dots, \mathbf{x}_{2020}) \in \mathbb{R}^{n \times m}. \quad (2)$$

Here, n is twice the number of grid nodes defined in PINNs and m is the number of snapshots, with a time interval of one year between them. DMD calculates the eigenvector and eigenvalue of the best-fit linear operator \mathbf{A} , which is associated with the data via $\mathbf{X}' \approx \mathbf{A}\mathbf{X}$. Nevertheless, determining the matrix \mathbf{A} can be challenging when the dimension of \mathbf{X} are large. Consequently, DMD provides a rank-reduced representation of the matrix \mathbf{A} in terms of a POD-projected matrix $\tilde{\mathbf{A}} = \mathbf{U}^\dagger \mathbf{A} \mathbf{U}$. The columns of \mathbf{U} are the POD modes derived from the singular value decomposition of \mathbf{X} :

$$\mathbf{X} \approx \mathbf{U} \mathbf{\Sigma} \mathbf{V}^\dagger. \quad (3)$$

Here, the dagger represents the conjugate transpose, with $\mathbf{U} \in \mathbb{C}^{n \times r}$, $\mathbf{\Sigma} \in \mathbb{C}^{r \times r}$, and $\mathbf{V} \in \mathbb{C}^{m \times r}$. The scalar r is the rank of the reduced SVD approximation to \mathbf{X} . Then DMD calculates the eigenvector and eigenvalue of $\tilde{\mathbf{A}}$:

$$\tilde{\mathbf{A}} \mathbf{W} = \mathbf{W} \mathbf{\Lambda}. \quad (4)$$

The columns of \mathbf{W} are the eigenvectors, while the diagonal elements of $\mathbf{\Lambda}$ are the corresponding eigenvalues λ_k . DMD reconstruct the eigendecomposition of \mathbf{A} using \mathbf{W} and $\mathbf{\Lambda}$. The eigenvectors of \mathbf{A} are the columns of the matrix $\mathbf{\Phi}$:

$$\mathbf{\Phi} = \mathbf{X}' \mathbf{V} \mathbf{\Sigma}^{-1} \mathbf{W} \quad (5)$$

and the corresponding eigenvalues of each eigenvector (DMD modes) are λ_k . Utilizing λ_k , the frequency and the growth rate of the k_{th} mode are given by

$$\omega_k = \frac{\text{Im}(\ln \lambda_k)}{\Delta t}, \sigma_k = \frac{\text{Re}(\ln \lambda_k)}{\Delta t}. \quad (6)$$

Finally, the spatial-temporal flow field is decomposed into a linear combination of the dynamic modes:

$$\mathbf{x}(t) \approx \sum_{k=1}^r \phi_k \exp(\sigma_k + i\omega_k) b_k \quad (7)$$

where ϕ_k is the column of $\mathbf{\Phi}$ and b_k is the initial amplitude of each mode.

Corresponding author: Yufeng Lin, linyf@sustech.edu.cn

37 Following the above procedure, we have decomposed the core surface flow into several
 38 DMD modes. For each mode, the flow evolution appears as a wave motion and can be
 39 characterized by the period, the growth rate, and the initial amplitude of the mode. To
 40 demonstrate the spatial distribution of the Dynamic Mode Decomposition (DMD) modes,
 41 we present the time-averaged root mean square of the flow field for the first four dominant
 42 DMD modes in Figure 1. The morphology of the time-independent Mode 1 closely resembles
 43 the time-averaged flow. Mode 2 captures wave motion with a 45-year period, primarily
 44 concentrated in the Indian Ocean and polar regions. Mode 3 reflects wave motion with a 16-
 45 year period, prevalent in the Indian Ocean and North America. Mode 4 reflects wave motion
 46 with an 8-year period, prevalent in the Atlantic Ocean and Indian Ocean. The corresponding
 47 growth rates are $G_1 = 0.002$, $G_2 = -0.03$, $G_3 = -0.066$, and $G_4 = -0.002$, respectively.
 48 For comparison, the periods of the first four dominant magnetic secular variation modes
 49 provided in Xu and Lin (2023) are $T_1 = \infty$, $T_2 = 57.17$ yr, $T_3 = 15.64$ yr, $T_4 = 8.40$
 50 yr. The corresponding growth rates are $G_1 = -0.0072$, $G_2 = -0.0159$, $G_3 = -0.0236$,
 51 $G_4 = -0.0731$, respectively. The period deviation between the flow mode and the magnetic
 52 SV mode may be caused by the fact that the \overline{Br} or $\tilde{B}r$ also varies with time. Furthermore,
 53 we notice most modes possess a negative growth rate which means these modes are not
 54 stable and eventually disappear with time. The explanation is that the eigenvalues learned
 55 by DMD from noisy measurements tend to exhibit spurious damping (Baddoo et al., 2023),
 56 so the damping may not be real but simply due to the algorithm itself.

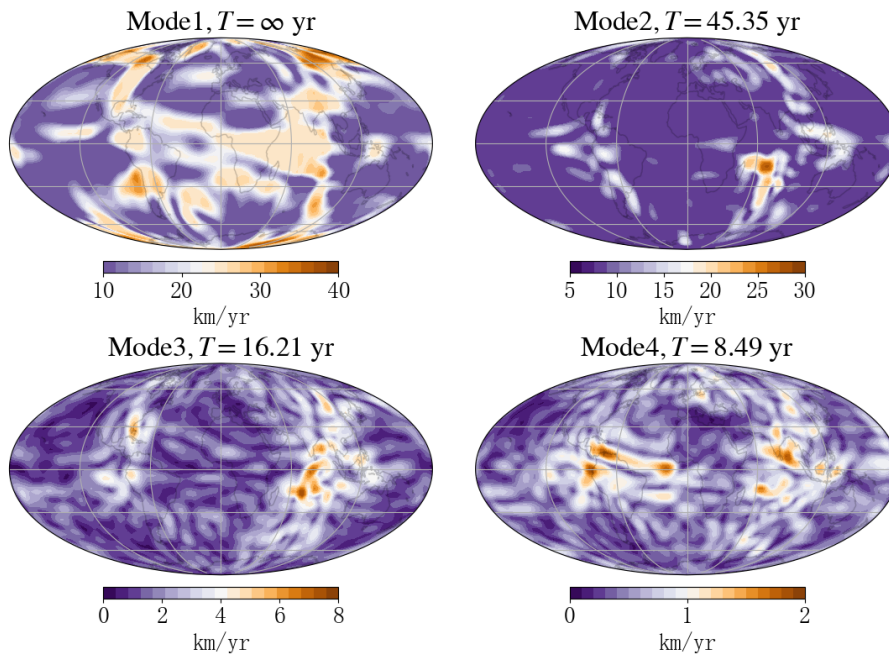


Figure 1. The DMD modes of the core-surface flow in Mollweide projection.

57 We are interested in determining if Mode 4 is related to equatorial SA pulses, given
 58 their similar periods and spatial distributions. To investigate this, we calculate the radial
 59 magnetic acceleration field for the first four DMD Modes, with the results presented in
 60 Figure 2. Figure 2a displays the magnetic acceleration derived from the combination of the
 61 first four DMD modes, while Figure 2d illustrates the corresponding azimuthal flow accelera-
 62 tion. Upon comparison with the CHAOS-7 model, Figure 2a essentially captures the main
 63 features of the magnetic acceleration. Any differences between Figure 2a and the CHAOS-
 64 7 model can be attributed to the SVD decomposition of the core-surface flow. Figure 2e
 65 represents the azimuthal flow acceleration field of Mode 4, and Figure 2b represents the

66 magnetic acceleration field generated by Mode 4. We observe a strong consistency between
 67 the phase of the acceleration field of Mode 4 and the corresponding phase of the magnetic
 68 acceleration field, suggesting that changes in the flow field primarily contribute to the mag-
 69 netic acceleration rather than the frozen flux effect. We refer to this phase consistency as
 70 CMAFA (Consistency between Magnetic Acceleration and Flow Acceleration). Next, we
 71 compute the flow acceleration field and magnetic acceleration field contributions from the
 72 other three modes, as displayed in Figure 2c and Figure 2f, respectively. It is evident that
 73 Mode 4 predominantly governs the flow motion in proximity to the vertical line, contributing
 74 nearly all the energy for both magnetic acceleration and flow acceleration. This significant
 75 contribution highlights the presence of the CMAFA phenomenon in this area.

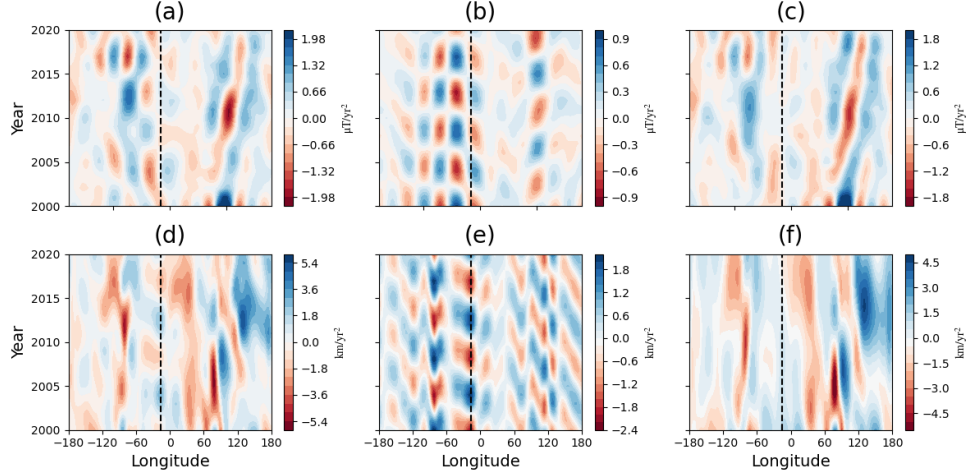


Figure 2. Time-longitude plots of equatorial radial magnetic secular acceleration and azimuthal flow acceleration. Plot (a) shows the SA signals derived from the combination of the first four DMD modes. Plot (b) shows the SA signals recovered from DMD Mode 4. Plot (c) represent the SA signals calculated from the combination of the other three modes. Corresponding azimuthal flow acceleration for each case is represented in Plot (d), Plot (e), and Plot (f), respectively.

References

- Baddoo, P. J., Herrmann, B., McKeon, B. J., Nathan, K. J., & Brunton, S. L. (2023). Physics-informed dynamic mode decomposition. *Proc. R. Soc.*, *479*. doi: 10.1098/rspa.2022.0576
- Xu, J., & Lin, Y. (2023). Dynamic mode decomposition of the geomagnetic field over the last two decades. *Earth and Planetary Physics*, *7*(1), 32-38. doi: 10.26464/epp2023026